

# Color-magnitude relations of late-type galaxies

Ruixiang Chang <sup>1</sup>; Shiyin Shen <sup>1</sup>; Jinliang Hou <sup>1</sup>; Chenggang Shu <sup>2,1</sup>; Zhengyi Shao <sup>1</sup>

## ABSTRACT

We use a large sample of galaxies drawn from the Sloan Digital Sky Survey (SDSS) and Two Micro All Sky Survey (2MASS) to present Color-Magnitude Relations (CMRs) for late-type galaxies in both optical and optical-infrared bands. A sample from SDSS Data Release 4 (DR4) is selected to investigate the optical properties. Optical-infrared colors are estimated from a position matched sample of DR4 and 2MASS, in which the photometric aperture mismatch between these two surveys is carefully corrected. It is shown that, after correcting the dust attenuation, the optical colors for faint galaxies (i.e.  $M_r > -21$ ) have very weak correlation with the luminosity, while the optical colors for bright galaxies (i.e.  $M_r < -21$ ) are redder for more luminous galaxies. All (optical, optical-infrared and infrared) colors show similar but stronger correlations with stellar mass than with absolute magnitude. The optical colors correlate more strongly with stellar mass surface density than with stellar mass, while optical-infrared and infrared colors show stronger correlations with stellar mass. By comparing the observed colors of our sample galaxies with the colors predicted by stellar population synthesis model, we find that massive late-type galaxies have older and higher metallicity stellar population than less massive galaxies. This suggests that CMRs for late-type galaxies are trends defined by the combination of stellar mean age and metallicity. Moreover, our results suggest that the stellar mean metallicity of late-type galaxy is mainly determined by its stellar mass, while the star formation history is mainly regulated by the stellar mass surface density.

*Subject headings:* Galaxies:evolution – Galaxies:photometry – Galaxies: stellar content

## 1. Introduction

It has long been known that early-type galaxies in nearby clusters exhibit a tight Color-Magnitude Relation (CMR), i.e. more luminous early-type galaxies have redder colors than less luminous ones (Baum 1959; Visvanathan & Sandage 1977; Bower et al. 1992), and this finding has been confirmed by later studies (Aragon-Salamanca et al. 1993; Stanford et al. 1995, 1998; Ellis et al. 1997; Kodama et al. 1998; Terlevich et al. 2001; Bernardi et al. 2003, 2005; Blanton et al. 2003a; Bell et al. 2004; Holden et al. 2004; Hogg et al. 2004; Cool et al. 2006; Chang et al. 2006). This relation has been mainly ascribed to the metallicity effect, either because more massive galaxies have

stronger binding energies so that the gas can be enriched to higher metallicity (Faber 1977; Dressler 1984; Arimoto & Yoshii 1987; Kodama & Arimoto 1997), or because larger ellipticals form at low redshift through major mergers between more massive, metal-rich disk systems (Kauffmann & Charlot 1998; De Lucia et al. 2004; Kang et al. 2005).

However, the case for late-type galaxies is much more complicated partially because of the influence of on-going star formation and the effect of dust attenuation. Almost thirty years ago, Visvanathan & Griersmith (1977) find that early-type spiral galaxies (S0/a to Sab) in the Virgo cluster exhibit very similar optical CMR to that of E/S0 galaxies, i.e. brighter spirals show redder colors, except that the former has a much larger scatter. Based on a large sample from Sloan Digital Sky Survey (SDSS, York et al. 2000), Blanton et al. (2003b) investigate the broadband optical prop-

<sup>1</sup>Shanghai Astronomical Observatory, 80 Nandan Road, Shanghai, China, 200030

<sup>2</sup>Shanghai Normal University, Road, Shanghai, China, 200030

erties for concentrated galaxies (fitted Sersic index  $n > 3$ ) and exponential galaxies ( $n < 1.5$ ) and find that exponential galaxies have a less tight, but undeniable optical CMR. Baldry et al. (2004) analyze the bimodal color-magnitude distribution of SDSS galaxies and find that both red and blue-distribution galaxies can be well fitted by a straight line plus a  $\tanh$  function. In other words, the low-luminosity blue-distribution galaxies ( $M_r > -19$ ) show a shallower CMR slope than high-luminosity galaxies. However, these works are all limited to the optical bands.

Tully et al. (1998) investigate global extinction in spiral galaxies and establish optical-IR CMRs for spirals after correction for dust attenuation. Peltier & de Grijs (1998) determine an optical-infrared CMR ( $I - K$  vs.  $M_K$ ) for spiral galaxies. They find the CMR is very tight and its slope is steeper than that for elliptical and S0 galaxies. This result is consistent with early studies (e.g. Wyse 1982; Tully et al. 1982; Mobasher et al. 1986). Using stellar population synthesis (SPS) models, they conclude that faint spiral galaxies have both a younger age and a lower metallicity than bright spirals. Bell & de Jong (2000) have compiled a sample of 121 low-inclination spiral galaxies with radially resolved optical and near-infrared photometry. By comparing the available photometry with the SPS model colors, they found that the star formation history of a galaxy (as probed by its age, metallicity and gas fraction) strongly correlates with its surface brightness and magnitude. These results are confirmed by Macarthur et al. (2004). However, all those early studies are limited to small galaxy samples since it is difficult to get large and homogeneous optical and infrared photometric samples simultaneously.

On the other hand, the interpretation of these observed CMRs is still a challenge for semi-analytic models. van den Bosch (2002) and Bell et al. (2003) find that there is significant discrepancy between the predictions of semi-analytic models and the data. The observations show that brighter spiral galaxies are redder than fainter ones, while the models predict that fainter spirals should be slightly redder than bright spirals. Recently, Kang et al. (2005) introduce a semi-analytic model based on high-resolution N-body simulations and compare their model predictions with the observed

bimodal distribution in the color-magnitude diagram found by Baldry et al. (2004). They find that the prediction for the red branch is very close to the observations, but for the blue part, the predicted colors of luminous spirals are bluer and those of less luminous spirals are redder than observations. All these results suggest that the implied physics of gas accretion and feedback during the formation and evolution of spiral galaxies are still not well understood (van den Bosch 2000; Bell et al. 2003).

It should be pointed out that the comparison presented by Kang et al. (2005) is only limited to the color ( $u - r$ ), which is very sensitive to dust attenuation. Furthermore, the degeneracy between stellar age and metallicity for optical colors complicates further investigations for the star formation history of late-type galaxies. Thus, there is still a long way to go before getting robust conclusions. Since the combination of optical and near-infrared broad-band colors can partially break age-metallicity degeneracy, it is important to establish observationally the CMRs in both optical and near-infrared bands for late-type galaxies based on a large homogenous sample.

The SDSS and Two Micron All Sky Survey (2MASS, Jarrett 2000a,b) have already created the largest well-defined sample of galaxies with well-measured optical and infrared photometry to date. Recently, we have analyzed the optical and infrared color properties for early-type galaxies after correcting the aperture mismatch between these two magnitude systems (Chang et al. 2006). This paper is a complementary study of Chang et al. (2006). Here the samples are selected for late-type galaxies. One of our aims is to establish optical, optical-infrared and infrared CMRs for late-type galaxies by using the largest homogeneous samples up-to-date.

To derive the optical-infrared colors, we adopt the method presented in Chang et al. (2006) and correct SDSS magnitudes to the aperture where 2MASS magnitudes are measured. For the purpose of minimizing the different dust attenuation caused by different inclinations, the galaxies in our sample are limited to face-on spirals. We also calculate the emission-line-free colors by comparing the magnitude difference before and after removing the emission lines from the spectra. With these carefully corrected optical and optical-infrared col-

ors, we compare the correlations between colors and absolute magnitude, stellar mass and stellar mass surface density and try to distinguish which parameter mainly determines the color properties for late-type galaxies. Moreover, by comparing the colors of our sample galaxies with those of SPS models, we investigate the stellar populations of spiral galaxies and their implications on star formation processes in late-type galaxies.

The outline of this paper is as follows. Section 2 describes the way of selecting sample galaxies and the photometric quantities used in the paper. Section 3.1 presents the method to do the photometric aperture corrections. The magnitude corrections for emission-line contamination is shown in Section 3.2. Section 4 is the main part of the paper, where we present various correlations between colors and absolute magnitudes, stellar mass and stellar mass surface density and their comparisons. Section 5 describes the SPS models and the model predictions for stellar populations of spiral galaxies. Finally, in Section 6 we summarize the main results of this paper.

## 2. The data and samples

The data used in this paper is mainly taken from Data Release 4 of the SDSS (York et al. 2000; Stoughton et al. 2002, hereafter EDR; Adelman-McCarthy et al. 2006). In particular, we use the Main Galaxy Sample in the New York University Value-Added Galaxy Catalog (NYU-VAGC), which is based on the SDSS database, but with an independent set of enhanced reductions (Blanton et al. 2005). From this catalog, we take spectroscopic redshift and photometric quantities, including Petrosian magnitudes, K-corrections, axis ratio ( $b/a$ ) from the exponential fitting ( $a$  and  $b$  are the semimajor and semiminor axes) and  $fracDev_r$ . The parameter  $fracDev_r$  is obtained by taking the best-fit exponential and de Vaucouleurs fit to the surface brightness profile, finding the linear combination of the two that best fits the image, and storing the fraction contributed by the de Vaucouleurs fit. We also take the quantities from ProfMean, the azimuthally averaged surface brightness in a series of fixed circular annuli (see table 7 in EDR), which are used to make the aperture correction for the optical-infrared colors (see section 3.1).

The 2MASS is a ground-based, near-infrared imaging survey of the whole sky and its Extended Source Catalog (XSC) contains nearly 1.6 million galaxies (Jarrett et al. 2000a,b). The infrared magnitudes are taken from extended source catalog (XSC) of 2MASS. In section 3.1, we will describe how to estimate the optical-infrared colors.

Conversion from apparent magnitude  $m$  to absolute magnitude  $M$  depends on the adopted cosmology and the K-correction:

$$M = m - 5 \log[D_L(z, \Omega_M, \Omega_\Lambda)] - 25 - K(z), \quad (1)$$

where  $D_L$  is the luminosity distance in unit of Mpc and  $K(z)$  is the K-correction. We assume the standard cosmology with  $\Omega_M = 0.3$ ,  $\Omega_\Lambda = 0.7$  and  $H_0 = 70 \text{ km s}^{-1} \text{ Mpc}^{-1}$  to calculate luminosity distance. We use SDSS  $r$ -band Petrosian magnitude and calculate  $M_r$  at redshift  $z = 0$ . K-corrections for magnitudes in the  $g$ ,  $r$ ,  $i$ ,  $z$  bands (and  $J$ ,  $H$ ,  $K$  bands if needed) are taken from NYU-VAGC (Blanton et al. 2003a; Blanton et al. 2005). Stellar masses of galaxies are taken from <http://www.mpa-garching.mpg.de/SDSS> (see details in Kauffmann et al. 2003a).

Sample galaxies are selected from Main Galaxy Sample in the NYU-VAGC (Blanton et al. 2005). We adopt the  $r$ -band morphology indicator  $fracDev_r$  to select late-type galaxies with criteria  $fracDev_r < 0.5$ , which means that the surface brightness of selected galaxy is more likely to be expressed by exponential profile. Adopting  $fracDev$  parameter has the advantage of seeing and inclination correction during the profile fitting (Bernardi et al. 2005). From this criteria, our sample contains 154,870 late-type galaxies.

We further restrict our sample with the condition  $b/a > 0.75$  so as to select nearly face-on galaxies based on two considerations. Firstly, edge-on galaxies are more dust-attenuated and reddened than face-on systems (Tully et al. 1998; Xiao et al. 2006). This effect will introduce extra dispersion into the CMRs. In other words, by selecting face-on galaxies, we can minimize the effects of dust attenuation caused by different inclination of the spiral disks. Secondly, the isophoto aperture of the high axis-ratio galaxies is nearly circular. In this case, the SDSS ProfMean measured in circular radii can be properly used to make the aperture correction of optical-infrared colors with enough accuracy. After this, the number of late-

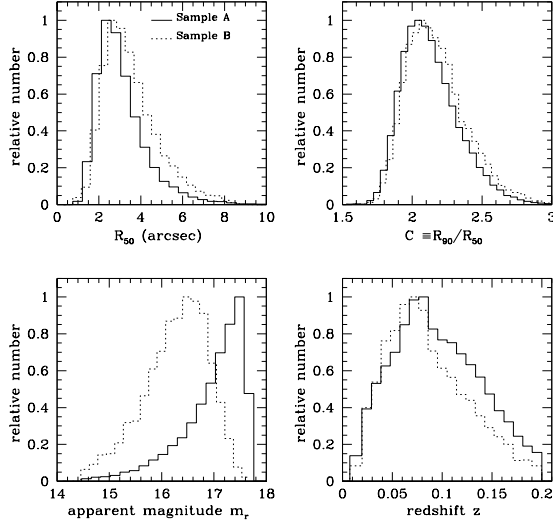


Fig. 1.— Distributions of several quantities for the galaxies in Sample A (solid lines) and Sample B (dotted lines), including  $R_{50}$ (arcsec), concentration  $C = R_{90}/R_{50}$ , r-band apparent magnitude  $m_r$  and redshift  $z$ .

type galaxies is reduced to 45,033.

Furthermore, we restrict our sample to galaxies in the redshift range  $0.01 < z < 0.2$ . The lower limit is to reduce the uncertainty using the redshift as distance estimator. The upper limit is to lower the uncertainties on K-corrections for the magnitudes and to reduce the possible color evolution with redshift. Finally, the number of galaxies is further reduced to 40,987. We denote this sample as Sample A and use it to investigate the optical CMRs.

The NYU-VAGC also contains a matched sample between SDSS and 2MASS XSC. This sample is obtained by positionally matching sources observed by 2MASS to galaxies in the ‘main’ spectroscopic sample of the SDSS within  $3\text{arcsec}$ . We select all the galaxies in sample A with 2MASS match to create Sample B. There is no cut in neither  $m_K$  nor surface brightness in K-band. The final number of galaxies in Sample B is 9,930. Sample B is used to investigate the optical-infrared and infrared CMRs.

Fig. 1 plots histograms of several quantities for

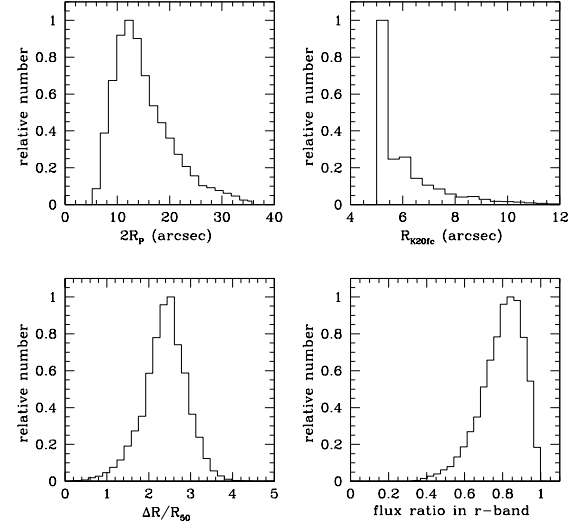


Fig. 2.— Histograms of several quantities relevant to do aperture corrections for galaxies in Sample B, including two times Petrosian radius in the  $r$ -band  $2R_P$  (from SDSS), the isophotal radius  $R_{k20fc}$  (from 2MASS),  $\Delta R/R_{50}$  and the  $r$ -band flux within  $R_{k20fc}$  divided by the Petrosian flux.

the galaxies in Sample A (solid lines) and Sample B (dotted lines), including  $R_{50}$ (arcsec), concentration  $C \equiv R_{90}/R_{50}$  ( $R_{90}$  and  $R_{50}$  are the radii including 50% and 90% of the Petrosian fluxes), r-band apparent magnitude  $m_r$  and redshift  $z$ . As we can see from the top-right panel of Fig. 1, most of the sample galaxies have  $C < 2.6$ , consistent with the early studies of the morphology separation with parameter  $C$  (e.g. Strateva et al. 2001). Compared with Sample A, the galaxies in Sample B are biased to be apparently bright, large and to lower redshifts. This is due to the fact that 2MASS is much more shallow than SDSS.

### 3. Corrections for magnitudes

#### 3.1. Aperture corrections

In order to estimate the optical-infrared colors, it is important that both SDSS and 2MASS magnitudes are measured within the same aperture. We adopt the same method as that in Chang et al. (2006) to do aperture corrections for the mag-

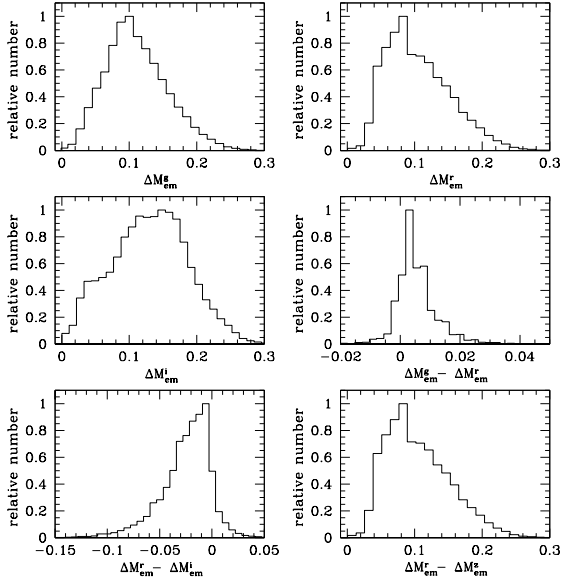


Fig. 3.— Histograms of emission-line corrections for magnitudes in  $g$ -band (left-top),  $r$ -band (right-top),  $i$ -band (left-meddle) and colors  $g - r$  (right-middle),  $r - i$  (left-bottom) and  $r - z$  (right-bottom) in the fiber.

nitudes, i.e. to correct SDSS magnitudes to the aperture where the 2MASS magnitudes are measured.

There are several sets of magnitudes provided in the 2MASS XSC. In this paper, we use the isophotal fiducial magnitudes, which are measured within the circular aperture corresponding to a surface brightness of 20.0 mag arcsec $^{-2}$  in the  $K_s$ -band (the aperture is denoted as  $R_{K20fc}$ ). SDSS provides the azimuthally averaged surface brightness in a series of circular annuli, i.e. ProfMean. We calculate  $g, r, i, z$  magnitudes that are matched to the 2MASS measurements by interpolating the cumulative radial surface brightness profile in each SDSS band at the corresponding isophotal radius  $R_{K20fc}$  (using the recommended approach in section 4.4.6.2 of EDR). The derived magnitude in  $r$ -band  $m_K^r$  is used to estimate the optical-infrared colors throughout this paper. The average value of magnitude correction in the  $r$ -band for aperture mismatch is 0.26.

Fig. 2 plots the distribution of several quantities for galaxies in Sample B, including two times

Petrosian radius in the  $r$ -band  $2R_P$  (from SDSS)<sup>3</sup>, the isophotal radius  $R_{K20fc}$  (from 2MASS), the aperture mismatch  $\Delta R/R_{50,r} = (2R_P - R_{K20fc})/R_{50,r}$  and the ratio between the  $r$ -band flux within  $R_{K20fc}$  and the Petrosian flux. It can be seen that the aperture mismatch between SDSS and 2MASS is quite large. However, more than half of the Petrosian flux is already contained within  $R_{K20fc}$  for most of galaxies.

### 3.2. Emission-line corrections

Since late-type galaxies have on-going star formation, emission lines from HII regions have significant contributions to the observed magnitudes. However, SPS models generally do not include contributions from emission lines. Therefore, it is necessary to correct the emission-line contaminations for the magnitudes when we compare the predicted colors from stellar population models with the observed ones (as what we will do in Section 5).

We use the magnitudes computed from the galaxy spectra to correct emission-line contaminations for the magnitudes. The magnitude difference estimated from the spectra before and after removing the emission lines (denoted as  $\Delta M_{em}$ ) represents the correction inside the fiber. Assuming the contribution of emission lines to the total magnitude equals to that in the fiber<sup>4</sup>, the sum of Petrosian magnitude and  $\Delta M_{em}$  can be regarded as emission-free magnitude and the colors estimated from this set of magnitudes are treated as emission-line-free colors.

Fig. 3 presents distributions of emission-line corrections for magnitudes and colors in the fiber. It can be seen that, although the corrections for the magnitudes are small, emission lines do influence the colors.

<sup>3</sup>The  $r$ -band  $2R_P$  is the aperture to which the Petrosian magnitudes are integrated, see EDR

<sup>4</sup>This assumption may not always be correct. Since the outer part of spirals has bluer colors, which implies a higher average specific star formation rate ( $SFR/M_*$ ) than that in the inner part, our method may **underestimate** the emission-line contamination. On the other hand, due to the contribution of AGN in the nuclear region of massive galaxies, our method may **overestimate** the emission-line contamination.

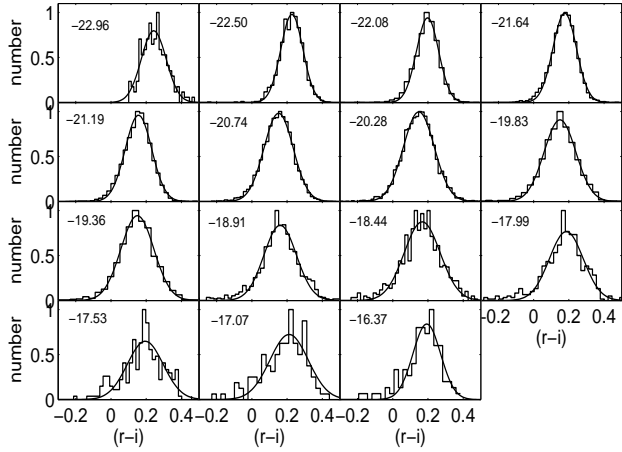


Fig. 4.— Histograms of  $r - i$  (after emission-line and dust corrections) for galaxies in Sample A at different bins. The solid curves are the best-fit results for Gaussian functions. The median value of  $M_r$  in each bin is shown as the number in each panel.

### 3.3. dust corrections

Although dust attenuation in face-on late-type galaxy is not expected to be large, it may have significant effect on the colors. It would be helpful if the influence of dust can be estimated and accounted for.

Kauffmann et al. (2003a) has already obtained the dust attenuation in the z-band,  $A_z$ , for SDSS galaxies. They use the 4000Å break strength and the Balmer absorption line index  $H\delta_A$  to constrain the best star formation history for one galaxy. The dust extinction is estimated by comparing observed imaging  $g - r$  and  $r - i$  colors to model-predicted colors. We adopt  $A_z$  from <http://www.mpa-garching.mpg.de/SDSS> for our sample galaxies. The median value of  $A_z$  for Sample A and B is 0.21 mag and 0.24 mag, respectively. By adopting the standard attenuation curve of the form  $\tau_\lambda \propto \lambda^{-0.7}$ , we can estimate the dust attenuation in other bands. We refer "colors" as these emission-line-free and dust-free colors throughout this paper if there is no special notation.

It should be pointed out that our method to correct the effect of dust attenuation may not be accurate for individual galaxy. However, the results for the global trends are robust. Indeed,

Obrić et al. (2006) find evidences to confirm that the estimates of  $A_z$  are related to the galaxy dust content.

## 4. Results

### 4.1. Color-magnitude relations

In this section, we use Sample A (only from SDSS) to investigate optical CMRs and Sample B (a matched sample of SDSS and 2MASS) for optical-infrared and infrared CMRs. The optical colors ( $g - r$ ,  $r - i$ ,  $r - z$ ) are estimated from the Petrosian magnitudes. The optical-infrared colors ( $r - J$ ,  $r - K$ ) are derived using the aperture-corrected magnitudes in the r-band and the isophotal fiducial magnitudes from 2MASS. The infrared color  $J - K$  are estimated from the isophotal fiducial magnitudes from 2MASS. All the magnitudes are corrected for Galactic foreground extinction and K-correction.

The galaxies in each sample are divided into 15 bins according to their absolute magnitudes in the r-band,  $M_r$ . We choose equal intervals of  $M_r$  in each bin and make sure that each bin contains more than 100 galaxies. The colors are corrected for dust extinction by calculating a median value of  $A_z$  in each bin since the estimated  $A_z$  for individual galaxy is model-dependent but the general trend is reliable. It is found that the median  $A_z$  in luminous bin is larger than less luminous bin and the median  $A_z$  is slightly negative for faint galaxies ( $M_r > -19$ ).

Fig. 4 plots histograms of  $r - i$  (after emission-line and dust corrections) for galaxies in Sample A at different bins. The median value of  $M_r$  in each bin is shown as the number in each panel. It is clear that the distributions of  $r - i$  can be well approximated by Gaussian functions, which are plotted by solid curves obtained from maximum likelihood estimations. The distributions of other colors show similar behaviors. Therefore, we can assume that the color distributions in each bin can be expressed by a Gaussian function

$$P[C(M_r)] = \frac{1}{2\pi\sigma(M_r)} \exp\left\{-\frac{[C(M_r) - \bar{C}(M_r)]^2}{2\sigma^2(M_r)}\right\}, \quad (2)$$

which is characterized by the mean  $\bar{C}(M_r)$  and the dispersion  $\sigma(M_r)$ . The best estimations for  $\bar{C}(M_r)$  and  $\sigma(M_r)$  are listed in Table 1. Further

Table 1: color-magnitude relations

$M_r$	$g - r$		$r - i$		$r - z$		$M_r$	$r - J$		$r - K$		$J - K$	
	$\bar{C}$	$\sigma$	$\bar{C}$	$\sigma$	$\bar{C}$	$\sigma$		$\bar{C}$	$\sigma$	$\bar{C}$	$\sigma$	$\bar{C}$	$\sigma$
(1)	(2)	(3)	(4)	(5)	(6)	(7)	(8)	(9)	(10)	(11)	(12)	(13)	(14)
-16.37	0.42	0.12	0.19	0.08	0.31	0.16	-18.58	1.52	0.24	2.46	0.29	0.91	0.18
-17.07	0.45	0.13	0.21	0.11	0.33	0.22	-19.08	1.49	0.19	2.35	0.26	0.86	0.19
-17.53	0.42	0.10	0.19	0.10	0.35	0.18	-19.37	1.52	0.16	2.47	0.21	0.93	0.17
-17.99	0.41	0.09	0.19	0.10	0.31	0.20	-19.66	1.52	0.17	2.44	0.21	0.92	0.13
-18.44	0.42	0.10	0.17	0.10	0.33	0.20	-19.96	1.55	0.16	2.46	0.19	0.93	0.13
-18.91	0.42	0.09	0.16	0.09	0.34	0.18	-20.26	1.57	0.17	2.51	0.22	0.94	0.14
-19.36	0.43	0.08	0.15	0.09	0.33	0.17	-20.57	1.57	0.16	2.53	0.20	0.94	0.13
-19.83	0.43	0.09	0.15	0.09	0.35	0.16	-20.86	1.59	0.14	2.55	0.20	0.96	0.15
-20.28	0.44	0.09	0.15	0.09	0.36	0.15	-21.15	1.59	0.13	2.55	0.18	0.95	0.14
-20.74	0.43	0.09	0.15	0.08	0.36	0.14	-21.45	1.61	0.14	2.59	0.18	0.97	0.14
-21.19	0.43	0.08	0.16	0.08	0.37	0.13	-21.75	1.65	0.12	2.62	0.16	0.98	0.13
-21.64	0.44	0.07	0.18	0.07	0.41	0.13	-22.05	1.70	0.13	2.69	0.16	0.98	0.12
-22.08	0.47	0.08	0.20	0.06	0.45	0.13	-22.34	1.76	0.13	2.76	0.16	0.99	0.14
-22.50	0.50	0.07	0.23	0.06	0.51	0.13	-22.63	1.81	0.13	2.82	0.14	1.00	0.12
-22.96	0.60	0.08	0.29	0.07	0.62	0.12	-22.96	1.87	0.13	2.86	0.14	0.99	0.12

tests show that main results do not change if a narrower redshift range (such as  $0.01 < z < 0.1$ ) is used to construct the sample.

The results for CMRs are plotted in Fig. 5, where the filled square represents the value of the color (y-axis) as a function of  $M_r$  (x-axis) in each bin, the error bar represents the dispersion  $\sigma(M_r)$ . We also show the results after emission-line corrections but without dust corrections as open squares without error bars. To quantify the tightness of the relation, we define a parameter  $S = \frac{\Delta I}{\sigma}$ , where  $\Delta I$  is the difference between the mean color of the brightest bin and the faintest bin,  $\sigma$  is the average value for the color dispersions in 15 bins. Thus, higher  $S$  corresponds to tighter relation. The resulted  $S$  for the CMR is shown in the upper-left corner of each panel in Fig. 5.

It can be seen that dust attenuation contributes significantly to the observed CMRs. This is expected since luminous galaxy is more attenuated and reddened than less luminous object (Tully et al. 1998; Masters et al. 2003). After correcting the dust attenuation, the optical colors ( $g - r$ ,  $r - i$ ,  $r - z$ ) for faint galaxies (i.e.  $M_r > -21$ ) have very weak correlation with the luminosity, while the optical colors for bright galaxies (i.e.  $M_r < -21$ ) are redder for more luminous galaxies. This is con-

sistent with the results of Baldry et al. (2004), who also find a shallow CMR slope for the low-luminosity blue-distribution galaxies.

It is also shown that, after correcting dust attenuation, the optical-infrared ( $r - J$ ,  $r - K$ ) CMRs are still very tight. For infrared color ( $J - K$ ), a weak CMR is presented, in the sense that the color range  $\Delta I$  is comparable with the mean dispersion  $\sigma$ . Unfortunately, due to the fact that 2MASS is much more shallow than SDSS, there is no sufficient number of less luminous galaxies in Sample B to give the optical-infrared and infrared CMRs behavior at the fainter end.

#### 4.2. Correlations between colors and stellar mass

Stellar mass is another fundamental physical parameter for galaxies. Now, we turn to investigate the color-mass relations for late-type galaxies.

Again, we divide the galaxies into 15 bins according to their stellar mass  $M_*$  (which is in units of  $M_\odot$  throughout this paper) and fit the distribution of the color in each bin by a Gaussian function. The method to correct dust attenuation is the same as that in section 4.1. The best-fit mean of color and its dispersion in each bin are listed in

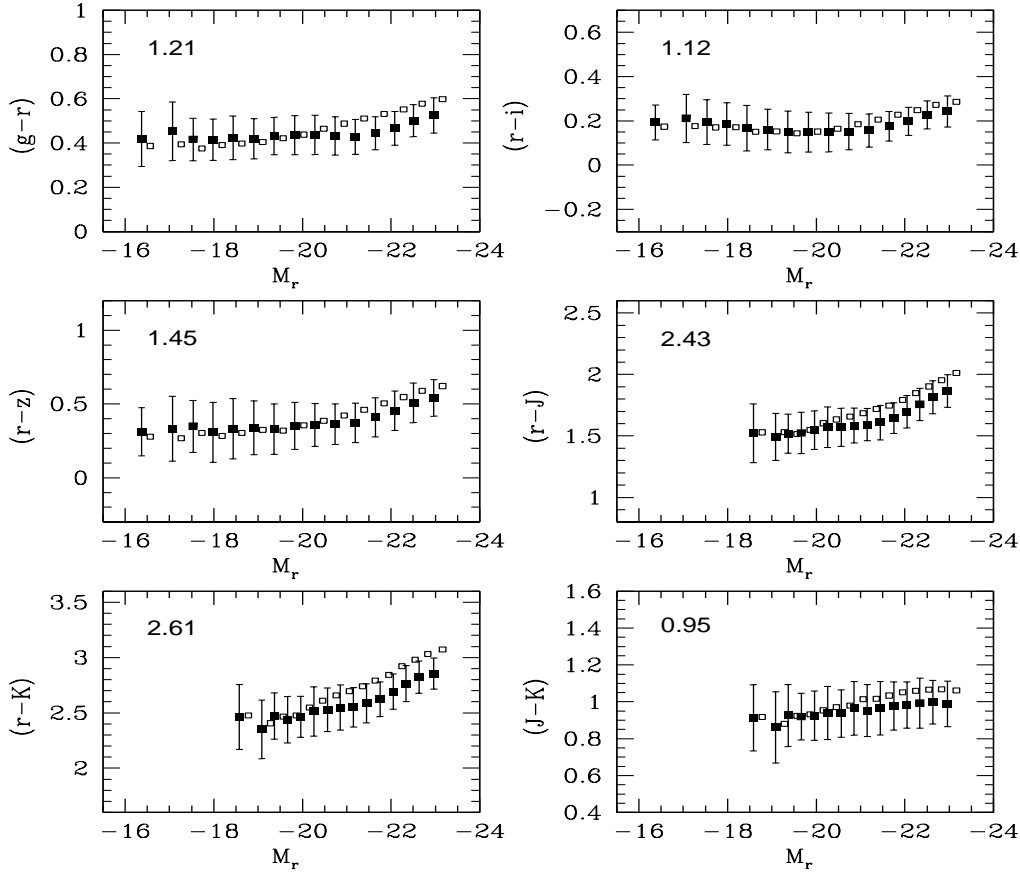


Fig. 5.— Color-magnitude relations, where the filled square represents the value for the emission-line-free and dust-free color (y-axis) as a function of  $M_r$  (x-axis) at each bin. The error bar represents the dispersion  $\sigma(M_r)$ . Open squares without error bars are the results after emission-line corrections but without dust corrections. The x-axis of open square is slightly shifted for clearness. The number in the upper-left corner of each panel shows the result of  $S = \frac{\Delta I}{\sigma}$  for each correlation (see text for details).

Table 2 and plotted in Fig. 6. The most remarkable feature of Fig. 6 is the tightness of correlation between optical-infrared color ( $r - J$ ,  $r - K$ ) and stellar mass, in the sense that  $\Delta I$  is nearly (if not more than) more than 3 times the mean color dispersion. We will discuss the implication of these results in Section 5.

It could be interesting to compare the CMRs with color-mass relations. The colors show similar but stronger correlations with stellar mass than luminosity. The colors in the reddest bins are redder and the colors in the bluest bins are bluer when mass is used instead of absolute magnitude. This is true for all wavelength bands. However, it's not

completely clear how much of the steeper slopes and tighter scatter in color-mass relations relative to CMRs is driven by the color dependence of stellar  $M/L$  values. Tremonti et al. (2004) also find that, when luminosity is used instead of mass, both dust and  $M/L$  variations act to smear out the turnover seen in the mass-metallicity relation at high metallicity.

#### 4.3. Correlations between colors and mass surface density

Stellar mass surface density, which describes how luminous mass is distributed along the disk, is another fundamental parameter for spiral galax-

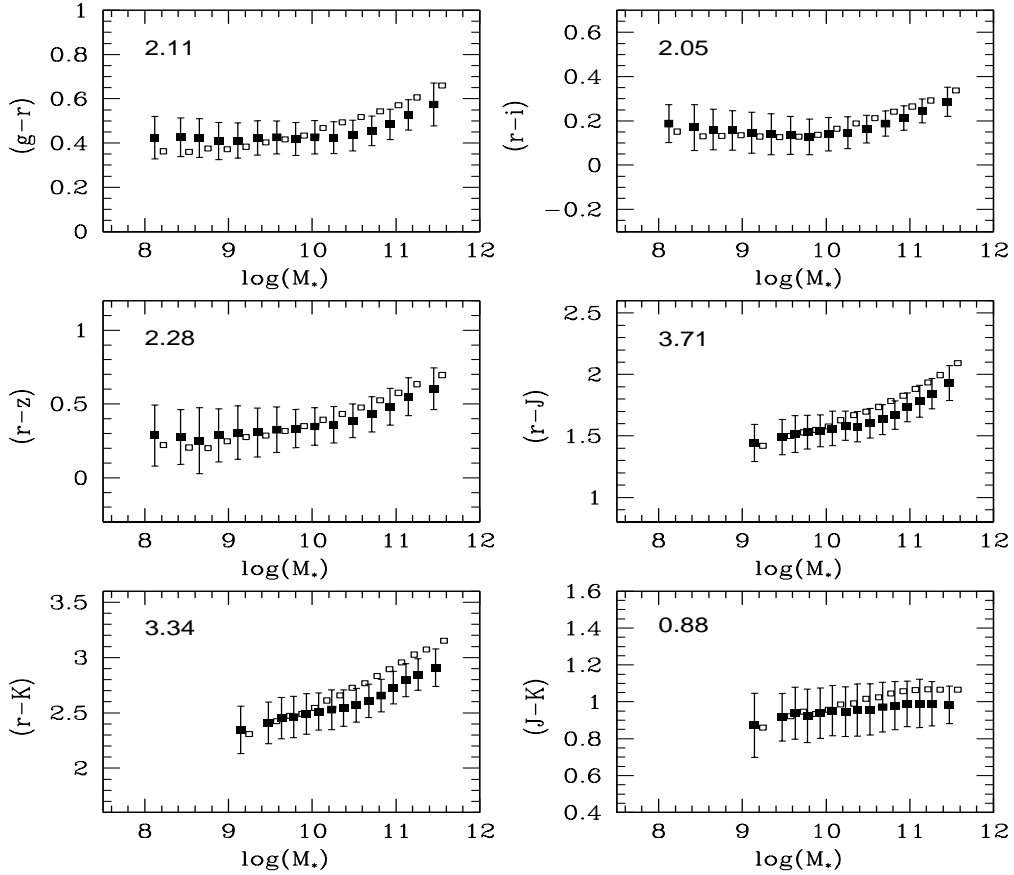


Fig. 6.— Correlations between colors and stellar mass. The caption is the same as that of Fig. 5.

ies. The half-light radius in the  $z$ -band and stellar mass yield the effective stellar mass surface density  $\mu_* = M_*/2\pi R_{50,z}^2$  (Kauffmann et al. 2005; Chang et al. 2006), which is in units of  $M_\odot \text{kpc}^{-2}$ . The results for color- $\mu_*$  relations are given in Table 3 and Fig. 7.

It can be seen that, both optical and optical-infrared colors show correlations with stellar mass surface density, i.e. galaxies with higher  $\mu_*$  have redder colors. This point is anyhow expected since high mass surface density corresponds to higher stellar mass for late-type galaxies (Shen et al. 2003). More interestingly, when  $\mu_*$  is used in place of  $M_*$ , the resulted  $S$  increases for optical color, while  $S$  decreases for optical-infrared and infrared colors. In other words, for late-type galaxies, the optical colors correlate more strongly with mass surface density than with stellar mass, while

optical-infrared and infrared colors show stronger correlations with stellar mass.

This is obviously different from what is obtained for early-type galaxies. Chang et al. (2006) have shown that, for elliptical galaxies, all galaxy colors correlate more strongly with stellar mass than with mass surface density, which suggests that the star formation history of nearby elliptical galaxies is primarily determined by the mass of the system. Since the age-metallicity degeneracy makes it difficult to directly deduce the property of stellar population from colors, it is instructive to break the age-metallicity degeneracy firstly, such as adopting the SPS models, and then discuss the implications of various correlations on the star formation histories (SFHs) for late-type galaxies.

Table 2: Correlations between colors and stellar mass.

$\log(M_*)$	$g - r$		$r - i$		$r - z$		$\log(M_*)$	$r - J$		$r - K$		$J - K$	
	$\bar{C}$	$\sigma$	$\bar{C}$	$\sigma$	$\bar{C}$	$\sigma$		$\bar{C}$	$\sigma$	$\bar{C}$	$\sigma$	$\bar{C}$	$\sigma$
(1)	(2)	(3)	(4)	(5)	(6)	(7)	(8)	(9)	(10)	(11)	(12)	(13)	(14)
8.12	0.42	0.10	0.19	0.09	0.29	0.21	9.15	1.44	0.15	2.35	0.21	0.87	0.17
8.43	0.43	0.09	0.17	0.10	0.28	0.19	9.48	1.49	0.14	2.41	0.19	0.92	0.13
8.65	0.42	0.09	0.16	0.09	0.25	0.22	9.63	1.51	0.15	2.45	0.19	0.94	0.14
8.88	0.41	0.08	0.16	0.09	0.29	0.18	9.78	1.53	0.14	2.46	0.19	0.92	0.14
9.11	0.41	0.08	0.15	0.09	0.31	0.18	9.93	1.54	0.13	2.49	0.18	0.94	0.14
9.35	0.42	0.08	0.14	0.09	0.31	0.17	10.08	1.56	0.14	2.51	0.17	0.95	0.14
9.57	0.43	0.07	0.13	0.09	0.33	0.15	10.23	1.58	0.12	2.53	0.18	0.95	0.14
9.80	0.42	0.07	0.13	0.08	0.33	0.13	10.38	1.58	0.12	2.54	0.16	0.95	0.14
10.03	0.43	0.08	0.14	0.08	0.35	0.13	10.53	1.60	0.12	2.57	0.15	0.96	0.14
10.26	0.42	0.07	0.15	0.07	0.36	0.12	10.67	1.63	0.12	2.61	0.15	0.97	0.13
10.48	0.43	0.07	0.16	0.06	0.39	0.11	10.82	1.67	0.12	2.66	0.15	0.98	0.13
10.71	0.46	0.07	0.19	0.06	0.43	0.12	10.97	1.73	0.12	2.73	0.15	0.99	0.12
10.93	0.48	0.07	0.21	0.06	0.48	0.13	11.12	1.78	0.13	2.80	0.15	0.99	0.13
11.15	0.53	0.07	0.25	0.05	0.55	0.13	11.27	1.84	0.12	2.85	0.14	0.99	0.12
11.45	0.57	0.10	0.29	0.07	0.60	0.14	11.47	1.93	0.14	2.91	0.17	0.98	0.10

 Table 3: Correlations between colors and stellar surface mass density  $\log(\mu_*)$ 

$\log(\mu_*)$	$g - r$		$r - i$		$r - z$		$\log(\mu_*)$	$r - J$		$r - K$		$J - K$	
	$\bar{C}$	$\sigma$	$\bar{C}$	$\sigma$	$\bar{C}$	$\sigma$		$\bar{C}$	$\sigma$	$\bar{C}$	$\sigma$	$\bar{C}$	$\sigma$
(1)	(2)	(3)	(4)	(5)	(6)	(7)	(8)	(9)	(10)	(11)	(12)	(13)	(14)
6.99	0.50	0.11	0.12	0.13	0.36	0.26	7.75	1.53	0.19	2.53	0.25	0.98	0.20
7.19	0.45	0.10	0.12	0.11	0.20	0.28	7.95	1.54	0.14	2.53	0.20	0.99	0.18
7.35	0.44	0.08	0.12	0.10	0.29	0.22	8.04	1.58	0.15	2.59	0.23	0.99	0.17
7.51	0.43	0.08	0.12	0.08	0.27	0.21	8.13	1.58	0.15	2.55	0.23	0.95	0.16
7.67	0.43	0.08	0.12	0.08	0.29	0.18	8.22	1.61	0.14	2.59	0.21	0.96	0.16
7.83	0.42	0.08	0.13	0.07	0.31	0.15	8.32	1.61	0.15	2.58	0.20	0.96	0.15
7.98	0.43	0.08	0.14	0.07	0.32	0.13	8.41	1.61	0.15	2.60	0.20	0.97	0.15
8.14	0.43	0.08	0.15	0.07	0.34	0.12	8.50	1.64	0.14	2.61	0.19	0.97	0.15
8.30	0.44	0.07	0.16	0.06	0.37	0.11	8.59	1.64	0.14	2.63	0.18	0.96	0.13
8.46	0.45	0.07	0.18	0.06	0.40	0.11	8.68	1.65	0.13	2.64	0.19	0.96	0.13
8.61	0.47	0.07	0.20	0.06	0.44	0.11	8.77	1.66	0.14	2.64	0.18	0.95	0.12
8.78	0.48	0.08	0.21	0.06	0.47	0.12	8.86	1.70	0.14	2.67	0.19	0.95	0.11
8.96	0.50	0.10	0.23	0.06	0.51	0.12	8.96	1.71	0.16	2.67	0.16	0.95	0.10
9.17	0.59	0.10	0.28	0.06	0.57	0.12	9.07	1.74	0.15	2.68	0.22	0.93	0.13
9.40	0.73	0.11	0.35	0.08	0.74	0.17	9.25	1.88	0.19	2.90	0.23	0.96	0.11

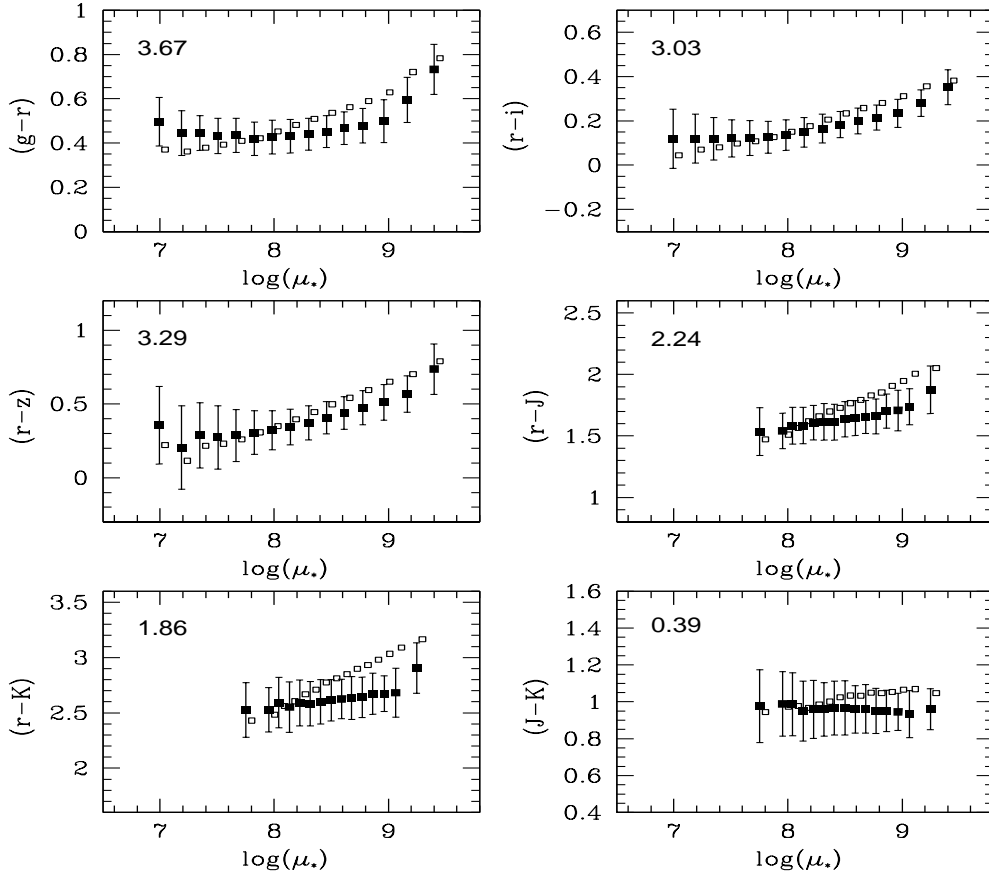


Fig. 7.— Correlations between colors and stellar mass surface density. The caption is the same as that of Fig. 5.

## 5. Stellar populations of late-type galaxies

Motivated by the work of Bell & de Jong (2000), we use a combination of optical and near-infrared broad-band colors for galaxies in our sample B to probe the stellar populations of late type galaxies. In other words, we generate a grid of model spectral energy distributions using SPS models and estimate the model parameters by matching all the available photometry of the sample galaxies to the colors predicted by the SPS models. By doing this, we are able to investigate the trends in the mean stellar age and metallicity as a function of stellar mass and mass surface density.

We adopt the SPS models of Bruzual & Charlot (2003). The universal initial mass function is taken from Chabrier (2003). The lower and

upper mass cut-offs are set as  $m_L=0.1M_\odot$  and  $m_U=100M_\odot$ , respectively. We use simplified SFHs and given metallicities to construct a grid of model colors. The star formation rate (SFR) is parameterized by:

$$\Psi(t) = \begin{cases} 0 & \text{if } t < t_{form} \\ Bte^{-t/\tau_{SF}} & \text{if } t_{form} \leq t \leq t_g, \end{cases} \quad (3)$$

where  $B$  is a normalization constant which determines the total mass of the stellar population,  $\tau_{SF}$  is the star formation timescale,  $t_g$  is the age of galaxy and is fixed as  $t_g = 12Gyr$ ,  $t_{form}$  characterizes the time delay for star formation. Under the above assumptions, the mean age of the stellar population  $\langle age \rangle$  is given by:

$$\langle age \rangle = \frac{\int_0^{t_g} (t_g - t) \psi(t) dt}{\int_0^{t_g} \psi(t) dt}. \quad (4)$$

Therefore, the mean age of stellar population is determined by the combination of  $\tau_{SF}$  and  $t_{form}$ . If  $t_{form} = 0$ , the youngest mean age given by none-negative  $\tau_{SF}$  is around 4Gyr, which corresponds to  $\tau \rightarrow \infty$  and the SFR increases with time. In this case, the stellar population is still too old to fit the colors of some observed blue galaxies. As an alternative, we assume a none-zero  $t_{form}$ , which insures that our models also include the youngest stellar populations. We assume  $t_{form} = 0.2\tau_{SF}$  during model calculations. This assumption is acceptable for two reasons. First, we focus only on the mean stellar age rather than details of SFH for each individual galaxy. Fixing the relation between  $\tau_{SF}$  and  $t_{form}$  will reduce the number of free parameters in the model. Second, SPS model has the advantage of giving robust relative ages and metallicities estimations (see discussions in Bell & de Jong 2000). We will emphasize the *relative trends* rather than the absolute values of ages and metallicities. Indeed, test calculations show that the main conclusions are not sensitive to either the adopted form of SFH or the assumption  $t_{form} = 0.2\tau_{SF}$ .

Thus, there are two free parameters in the model: metallicity and  $\tau_{SF}$ .  $\tau_{SF}$  progresses from 0 to 60Gyr ( $\tau_{SF} = 60$ Gyr corresponds to the upper limit for  $t_{form} = 12$ Gyr) smoothly. This results in the mean age of stellar population going from old to young. Firstly, we generate a model grid of single-burst stellar population (SSPs) for different metallicity by interpolating along the model metallicities. The range of the model metallicities is from  $0.005Z_{\odot}$  to  $2.5Z_{\odot}$ . Then, we generate a model grid for a number of  $\tau_{SF}$  values by integrating the SSPs with a given metallicity. These models provide a set of model colors  $C_{model,i}(<age>, Z)$  (where  $i$  denotes different color) for a range of SFHs and metallicity.

We match all the available colors of the galaxies to the colors predicted by the SPS models and estimate the model parameters using  $\chi^2$ -fitting. For each  $\tau_{SF}$  and metallicity  $Z$ , the corresponding  $\chi^2$  is given by:

$$\chi^2 = \sum_{i=1}^n \frac{(C_{model,i} - C_{obs,i})^2}{\sigma_i^2}. \quad (5)$$

where  $\sigma_i$  is the observed error for color  $i$ . The best model match ( $<age>, Z$ ) is the one with the minimum  $\chi^2$  value.

We use the observed  $g - r$ ,  $r - i$ ,  $r - z$ ,  $r - J$  and  $r - K$  colors in  $\chi^2$ -fitting. These colors are corrected by emission-line contamination and dust attenuation. Since the estimated  $A_z$  is model-dependent and may not be accurate for individual galaxy, we choose to correct an average trend of dust attenuation by fitting a linear relation between  $A_z$  and  $M_*$ , i.e. to estimate  $A_z$  from stellar mass. In general, massive galaxies have larger dust attenuation. The results for  $\chi^2$ -fitting show that there are about 5 percent of galaxies with the minimum  $\chi^2$  value located in either boundary of the model parameters  $\tau_{SF}$  and  $Z$ . We exclude these galaxies from further analysis below.

Fig. 8 plots the model predictions of ( $<age>, Z$ ) against stellar mass and mass surface density for galaxies in Sample B. To show the distribution more clearly, we plot sets of contours to indicate the positions within which different fraction of total number of galaxies is contained. We also adopt the Spearman rank-order test to quantify the significance of the relation and show the resulted correlation coefficient in the right corner of each panel. Fig. 8 shows that massive galaxies have older and higher metallicity stellar populations than less massive galaxies. In other words, not only the stellar metallicity but also the stellar mean age that contribute to the observed CMRs for late-type galaxies. To contrast, the CMRs of early-type galaxies are mainly ascribed to the metallicity effect: more luminous galaxies have redder colors because they have higher metallicities (Faber 1977; Dressler 1984; Arimoto & Yoshii 1987; Kodama & Arimoto 1997; Kauffmann & Charlot 1998; De Lucia et al. 2004; Kang et al. 2005).

The general trend for mass-metallicity relation found in this paper is similar to some earlier works (such as Peltier & de Grijs 1998; Bell & de Jong 2000). Moreover, gas-phase oxygen abundance in star-forming galaxy has already been found to be related to the luminosity or/and stellar mass of the system (Kobulnicky & Zaritsky 1999; Kobulnicky & Kewley 2004; Hammer et al. 2005; Liang et al. 2004; 2006 etc.). For comparison, we show the observed mass-metallicity relation presented by Tremonti et al.(2004) with three blue lines. To transfer  $12 + \log(O/H)$  to  $\log(Z/Z_{\odot})$ , we assume the metallicity  $Z$  can be represented by oxygen abundance and take the solar value as 8.8

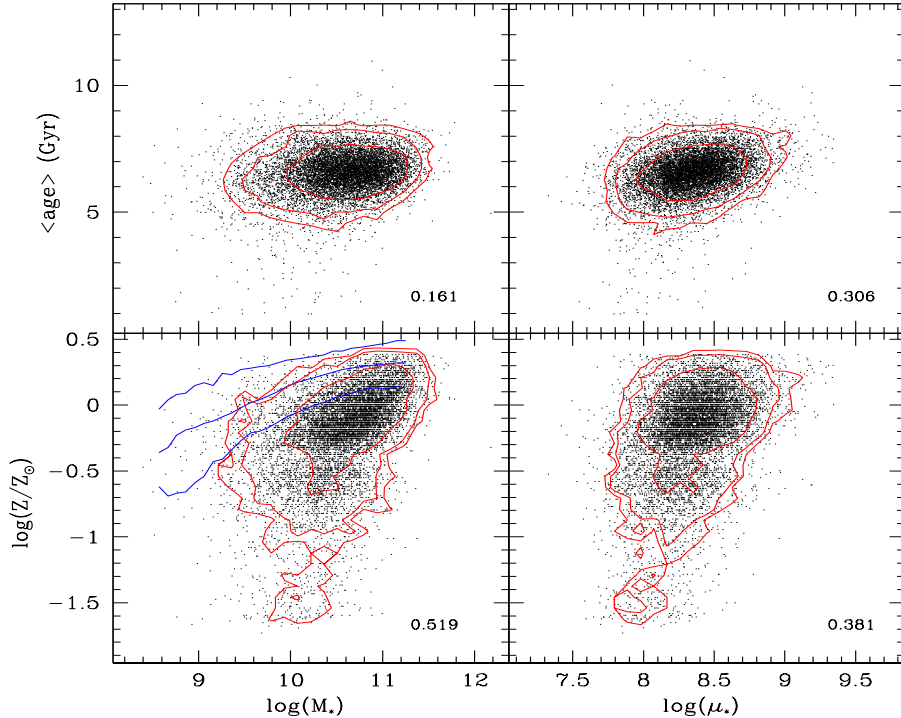


Fig. 8.— Model predictions of mean age ( $<age>$ ) and metallicity ( $Z$ ) against stellar mass and mass surface density for galaxies in Sample B. The set of contours indicates the positions within which how much fraction of total number of galaxies is contained. The levels of contours correspond to 68%, 90% and 95%, respectively. The number in the right corner of each panel shows the Spearman rank-order correlation coefficient. Three blue lines in bottom-left panel plot the observed range for the relation between stellar mass and gas-phase metallicity, which is taken from Table 3 in Tremonti et al.(2004). The solar  $12 + \log(O/H)$  is taken as 8.8 (Grevesse & Sauval 1998).

(Grevesse & Sauval 1998). Since the metallicity derived from SPS models is the mean value of the stellar population, it is reasonable that the model predicted metallicity is somewhat lower than that of Tremonti et al. (2004). As we can see, the general trend of our results deduced from the CMRs are consistent with their independent measurements from emission lines.

More interestingly, it can be seen (even by eye) that the metallicity correlates more strongly with  $M_*$  than  $\mu_*$ . We also find that the residuals from the age- $\mu_*$  relation do not correlate with  $M_*$ , while the residuals from the age- $M_*$  relation increase with  $\mu_*$ . All these suggest that the stellar mass of

late-type galaxy is the primary parameter to determine the mean metallicity of the system. This is probably, similar as early-type galaxy, because the stellar mass strongly correlates to the potential well of the galaxy and then determines the efficiency for ejecting the metals of the system. Tremonti et al. (2004) also interpret their results as strong evidence of both the ubiquity of galactic winds and their effectiveness in removing metals from galaxy potential wells.

On the other hand, the resulted mean stellar age  $<age>$  is more sensitive to  $\mu_*$  than  $M_*$ . It is also found that the residuals from the metallicity- $\mu_*$  relation strongly correlate with  $M_*$ , while the

residuals from the metallicity- $M_*$  relation have no correlation with  $\mu_*$ . In other words, our results suggest that mass surface density plays an more important role in regulating the star formation history of late-type galaxy than stellar mass. Indeed, some early studies already pointed out that the star formation history for late-type galaxies correlates more strongly with mass surface density than stellar mass (Bell & de Jong 2000; Kauffmann et al. 2003b; 2006). Kennicutt (1998) also shows that it is local (e.g. surface density) rather than global factors (e.g. stellar mass) that regulate the rate at which spiral galaxies form their stars at the present day.

## 6. Summary

We have collected two samples of face-on late-type galaxies to investigate the correlations between colors and absolute magnitude, stellar mass and stellar mass surface density. Sample A is selected from DR4 of SDSS and Sample B is a position matched sample between SDSS (DR4) and 2MASS. In order to correct the aperture mismatch between SDSS and 2MASS, we use the radial profile of SDSS galaxies and correct the SDSS magnitudes to the isophotal circular radius where the 2MASS magnitudes are measured. The emission-line contamination is corrected for the magnitudes by comparing the magnitudes computed from the spectra before and after removing the emission lines. We also correct dust attenuation by adopting  $A_z$  estimation plus an standard kind of attenuation curve. Moreover, we match the observed colors of our sample to the colors predicted by stellar population synthesis model and investigate their implications of the stellar populations. We find that:

1. The optical colors for faint galaxies (i.e.  $M_r > -21$ ) have very weak correlation with the luminosity, while the optical colors for bright galaxies (i.e.  $M_r < -21$ ) are redder for more luminous galaxies. The optical-infrared colors show tighter CMRs than optical ones.
2. All (optical, optical-infrared and infrared) colors show similar but stronger correlations with stellar mass than with absolute magnitudes.

3. The optical colors correlate more strongly with mass surface density than with stellar mass, while optical-infrared and infrared colors show stronger correlations with stellar mass.
4. By comparing the observed colors with SPS model colors, we find that massive galaxies have older and higher metallicity stellar populations than less massive galaxies. This suggests that the CMRs of late-type galaxies are the combined results of stellar mean age and metallicity.
5. It is also shown that the mean stellar metallicity is more sensitive to  $M_*$  than to  $\mu_*$ , while the mean stellar age is more sensitive to  $\mu_*$  than  $M_*$ . This suggests that the stellar metallicity is mainly determined by the mass of the system, while the star formation history of late-type galaxy is mainly regulated by mass surface density.

Our results are based on the homogeneous and large galaxies samples from SDSS and 2MASS to derive the CMRs for late-type galaxies in both optical and optical-infrared bands. Since the combination of optical and near-infrared broad-band colors contains more information on the star formation process, our observed results have provided strong constraints on the model descriptions for gas accretion and supernova feedback processes in late-type galaxies. Further comparisons between model predictions and observed data are needed to investigate the star formation histories for late-type galaxies.

## Acknowledgements

The authors thank the anonymous referee for his/her helpful suggestions to greatly improve this paper. We would like to thank Houjun Mo, Shude Mao, Guinevere Kauffmann, Eric Peng and Stéphane Charlot for useful discussions. We thank Jarle Brinchmann for providing the data of spectral magnitudes. This project is partly supported by NSFC 10403008, 10573028, 10333020, 10173017, NKBRSP 1999075404, Shanghai Municipal Science and Technology Commission No. 04dz05905.

Funding for the creation and distribution of the SDSS Archive has been provided by the Alfred P.

Sloan Foundation, the Participating Institutions, the National Aeronautics and Space Administration, the National Science Foundation, the U.S. Department of Energy, the Japanese Monbukagakusho, and the Max Planck Society. The SDSS Web site is <http://www.sdss.org/>.

The SDSS is managed by the Astrophysical Research Consortium (ARC) for the Participating Institutions. The Participating Institutions are The University of Chicago, Fermilab, the Institute for Advanced Study, the Japan Participation Group, The Johns Hopkins University, Los Alamos National Laboratory, the Max-Planck-Institute for Astronomy (MPIA), the Max-Planck-Institute for Astrophysics (MPA), New Mexico State University, University of Pittsburgh, Princeton University, the United States Naval Observatory, and the University of Washington.

## REFERENCES

Adelman-McCarthy J., et al, 2006, ApJS, 162, 38 (SDSS DR4 paper)

Aragon-Salamanca A., Ellis R.S., Couch W.J. & Carter D., 1993, MNRAS 262, 764

Arimoto N. & Yoshii Y., 1987, A&A 173, 23

Baldry I.K., Glazebrook K., Brinkmann J., et al., 2004, ApJ 600, 681

Baum W.A., 1959, PASP, 71, 106

Bell E.F., Baugh C.M., Cole S., et al., 2003, MNRAS 343, 367

Bell E.F., de Jong R.S., 2000, MNRAS 312, 497

Bell E.F., Wolf C., Meisenheimer K., et al., 2004, ApJ 608, 752

Bernardi M., Sheth R., Annis J., et al., 2003, AJ 125, 1882

Bernardi M., Sheth R., Nichol R.C., et al., 2005, AJ 129, 61

Blanton M.R. Brinkmann J, Csabai I., Doi M., Eisenstein D., Fukugita M., Gunn J.E., Hogg D.W. & Schlegel D.J., 2003a, AJ 125, 2348

Blanton M.R., Hogg D.W., Bahcall N.A., et al., 2003b, ApJ 594, 186

Blanton M.R., Schlegel D.J., Strauss, M.A., et al., 2005, AJ 129, 2562

Bower R.G., Laycey J.R., & Ellis R.S., 1992, MNRAS 254, 601

Bruzual G. & Charlot S., 2003, MNRAS 344, 1000

Chabrier G., 2003, ApJL 586, L133

Chang R.X., Gallazzi A., Kauffmann G., et al., 2006, MNRAS, 366, 717

Cool R.J., Eisenstein D.J., Johnston D., Scranton R., Brinkmann J., Schneider, D.P., Zehavi I., 2006, AJ, 131, 736

De Lucia G., Kauffmann G. & White S.D.M., 2004, MNRAS 349, 1101

Dressler A., 1984, ApJ 286, 97

Ellis R.S., Smail I., Dressler A., et al., 1997, ApJ 483, 582

Faber S.M., 1977, in Tinsley B.M., Larson R.B., eds, *The Evolution of Galaxies and Stellar Populations*. Yale Observatory, New Haven, p.157

Grevesse N. & Sauval A.J., 1998, Space Sci. Rev., 85, 161

Hammer F., Flores H., Elbaz D., et al., 2005, A&A, 430, 115

Hogg D., Blanton M., Brinchmann J., et al., 2004, ApJ 601, L29

Holden B.P., Stanford S.A., Eisenhardt P. & Dickinson M., 2004, AJ 127, 2484

Jarrett T.J., Chester T., Cutri R., et al., 2000a, AJ 119, 2498

Jarrett T.J., Chester T., Cutri R., et al., 2000b, AJ 120, 298

Kang X., Jing Y.P., Mo H.J., Borner G., 2005, ApJ, 631, 21

Kauffmann G. & Charlot S., 1998, MNRAS 294, 705

Kauffmann G., Heckman T., White S.D.M., et al., 2003a, MNRAS 341, 33

Kauffmann G., Heckman T., White S.D.M., et al., 2003b, MNRAS 341, 54

Kauffmann G., Heckman T., De Lucia G., et al., 2006, MNRAS, 367, 1394

Kennicutt R.C., 1998, ApJ 498, 541

Kobulnicky H.A. & Kewley L.J., 2004, ApJ, 617, 240

Kobulnicky H.A. & Zaritsky D., 1999, ApJ, 511, 118

Kodama T., Arimoto N., 1997, A&A 320, 41

Kodama T., Arimoto N., Barger A. & Aragon-Salamanca A., 1998, A&A 334, 99

Liang Y.C., Hammer F., Flores H., et al., 2004, A&A, 423, 867

Liang Y.C., Hammer F., Flores H., 2006, A&A, 447, 113

MacArthur L.A., Courteau S., Bell E., Holtzman J.A., 2004, ApJS, 152, 175

Masters K.L., Giovanelli R., Haynes M.P., 2003, AJ, 126, 158

Mobasher B., Ellis R.S., Sharples R.M., 1986, MNRAS 223, 11

Obreic M., Ivezić Z., Best P.N., et al., 2006 (astro-ph/0606344)

Peletier R.F. & de Grijs R., 1998, MNRAS 300, L3

Shen S.Y., Mo H. J., White, S. D. M., et al., 2003, MNRAS 343, 978

Stanford S.A., Eisenhardt P.R.M. & Dickinson M., 1995, ApJ 450, 512

Stanford S.A., Eisenhardt P.R.M. & Dickinson M., 1998, ApJ 492, 461

Stoughton C., et al., 2002, AJ 123, 485 (SDSS EDR paper)

Strateva I., Ivezić Z., Knapp G.R., et al., 2001, AJ 122, 1861

Terlevich A.I., Caldwell N. & Bpwer R.G., 2001, MNRAS 326, 1547

Tremonti C.A., Heckman T.M., Kauffmann G., et al., 2004, ApJ 613, 898

Tully R.B., Mould J.R., Aaronson M., 1982, ApJ 257, 527

Tully R.B., Pierce M.J., Huang J., Saunders W., Verheijen A.W., Witchalls P.L., 1998, ApJ, 115, 2264

van den Bosch F.C., 2002, MNRAS 332, 456

Visvanathan N. & Griersmith D., 1977, A&A, 59, 317

Visvanathan N. & Sandage A., 1977, ApJ 216, 214

Wyse R., 1982, MNRAS 199, 1

Xiao Q.B., Shao Z.Y., Shen S.Y., Mo H.J., Xia X.Y. Deng Z.G., in preparation

York D., et al., 2000, AJ 120, 1579